

NUMERICAL MODELING OF TETHER FORMATION IN VISCOUS LIPIDIC MEMBRANES

Diego S. Rodrigues^a, Roberto F. Ausas^b, Fernando Mut^a, Rainald Löhner^c and Gustavo C. Buscaglia^a

^a*Instituto de Ciências Matemáticas e de Computação, Universidade de São Paulo, Av. do Trabalhador são-carlense, 400, 13560-970 São Carlos, SP, Brazil, gustavo.buscaglia@icmc.usp.br*

^b*IBM Research, Brazil.*

^c*Computational Fluid Dynamics Group, George Mason University, MS 6A2, Fairfax, VA, USA.*

Keywords: Biological Membranes, Lipid Bilayer, Canham-Helfrich Energy, Boussinesq-Scriven Operator, Tangential Calculus, Finite Element.

Abstract. We present a finite element formulation to study the behavior of biological membranes governed by viscous and bending forces and subjected to area and volume constraints. The membrane is discretized by a surface mesh made up of planar triangles over which the Boussinesq-Scriven operator is solved to account for the viscous effects. A Laplace-Beltrami identity is used to compute the membrane curvature. A semi-implicit approach in which curvature and velocity are coupled, is used to improve stability of simulations. The area and volume constraints are accounted by considering suitable Lagrange multipliers. We focus on the formation of tethers in lipidic vesicles by means of externally applied forces. The simulation of a tether formation by pulling a small parcel of an originally spherical membrane was performed. The results were compared to the analytical solution of a cylindrical membrane under the influence of an external axial force. The agreement of the overall dynamics of the 3D tether with the exact solution of the idealized cylindrical tether is quite remarkable, indicating that the fundamental relaxation processes are adequately captured. Due to the large deformations suffered along the process a suitable adaptive re-meshing strategy is needed to preserve the mesh quality and thus robustness of computations, and to capture the tether's geometrical features. In our re-meshing procedure the new and the original meshes do not maintain a topological relation.

1 INTRODUCTION

Phospholipidic membranes are two-molecule-thick curved surface arrays of phospholipids (Alberts et al., 2010) that constitute the fundamental building material of cellular membranes at the micrometric scale. The physical properties of this two-dimensional material can be characterized as mostly homogeneous, with some amount of bending rigidity, with a large tangential elastic bulk modulus (area-preserving material) and a negligible tangential elastic shear modulus. On each one of the two lipid layers, tangential mobility of the amphiphilic molecules is so high that a better model for this material is that of a *surface fluid*. Even more, physics experiments have shown that its rheology corresponds to a *Newtonian surface fluid* (Harland et al., 2010, 2011), though with solid-like bending rigidity. Interest in studying viscous membranes like lipid bilayers arises from the ubiquitousness of such material in Nature and because in so doing one can explain why cells exhibit a wide variety of shapes configurations. Regarding the latter, the most classical example was provided by Canham (1970) who came up with an idea of the biconcave shape of the human red blood cell as a shape of a suitable minimum energy.

A salient phenomenon that takes place in phospholipidic bilayers is that, if a small part of a vesicle is pulled away by some localized force (using an optical trap, for example, as reported by Lee et al. (2008)) it carries with it a narrow bilayer tube (tether) that can be much longer than the vesicle itself and nanometric in diameter (Smith et al., 2004). The simulation of tether formation and extension aims at understanding the fundamental processes that govern this important phenomenon in biological membranes mechanics as theoretically discussed by Waugh (1982a) and Bozic et al. (1997) and also experimentally by Waugh (1982b).

In this article we describe a finite element method for phospholipidic membranes that is general enough (three-dimensional, unstructured, Eulerian) and robust enough to model tether formation and extension. It is coupled with an adaptive surface mesher so as to control mesh density and quality. Some numerical results illustrating the method's capability are reported.

2 MATHEMATICAL FORMULATION

2.1 The Boussinesq-Scriven operator

We consider the motion of a surface $\Gamma \subset \mathbb{R}^3$ governed by the following elastic energy proposed by Canham (1970) and Helfrich (1973)

$$\mathcal{E}(\Gamma) = \frac{c_{\text{CH}}}{2} \int_{\Gamma} \kappa^2, \quad (1)$$

where $\kappa = \kappa_1 + \kappa_2$ stands for the mean scalar curvature of Γ (κ_1 and κ_2 are the principal curvatures) and c_{CH} is a material dependent parameter. In differential geometry, equation (1) is known as Willmore energy (Willmore, 1993). The rheology of the interface Γ is governed by the Boussinesq-Scriven law (Scriven, 1960; Gross and Reusken, 2011). According to this, the stresses on the surface can be expressed as

$$\boldsymbol{\sigma} = \lambda (\nabla_{\Gamma} \cdot \mathbf{u}) \mathbb{P} + 2\mu D_{\Gamma} \mathbf{u}, \quad (2)$$

where λ and μ are surface viscosity coefficients, \mathbb{P} is the tangent projector onto Γ given by

$$\mathbb{P} = \mathbb{I} - \check{\mathbf{n}} \otimes \check{\mathbf{n}}, \quad (3)$$

$\check{\mathbf{n}}$ the normal to Γ and D_Γ is defined as

$$D_\Gamma \mathbf{u} = \frac{1}{2} \mathbb{P} (\nabla_\Gamma \mathbf{u} + \nabla_\Gamma \mathbf{u}^T) \mathbb{P}. \tag{4}$$

The surface gradient operator $\nabla_\Gamma f$ of a scalar function f defined on Γ is defined as $\mathbb{P} \nabla \hat{f}$ where \hat{f} is any regular extension of f to \mathbb{R}^3 . The surface gradient $\nabla_\Gamma \mathbf{w}$ of a vector field \mathbf{w} defined on Γ is defined as the matrix (Cartesian tensor)

$$\{\nabla_\Gamma \mathbf{w}\}_{ij} = \frac{\partial \hat{w}_i}{\partial x_j} = \{\nabla_\Gamma w_i\}_j, \tag{5}$$

where w_i is the i -th Cartesian component of \mathbf{w} and \hat{w}_i any regular extension of w_i to \mathbb{R}^3 .

In the limit of an area-preserving membrane ($\lambda \rightarrow +\infty$, frequently called *inextensible* membrane) the constraint $\nabla_\Gamma \cdot \mathbf{u}$ is satisfied. As occurs in bulk fluids, for surface fluids it can also be proved that there exists a *surface pressure* π_s (playing the role of minus an undetermined surface tension) such that

$$\lim_{\lambda \rightarrow +\infty} \lambda \nabla_\Gamma \cdot \mathbf{u} = -\pi_s, \tag{6}$$

so that in the inextensible limit the surface stress tensor reads

$$\boldsymbol{\sigma} = -\pi_s \mathbb{P} + 2 \mu D_\Gamma \mathbf{u}. \tag{7}$$

The bilinear form that expresses the virtual power along a virtual velocity field \mathbf{v} performed by the viscous stresses $\boldsymbol{\sigma}$ corresponding to an actual velocity field \mathbf{u} and surface pressure π_s is given by

$$\begin{aligned} \mathcal{W}((\mathbf{u}, \pi_s), \mathbf{v}) &= \int_\Gamma \boldsymbol{\sigma} : D_\Gamma \mathbf{v} = \\ &= \int_\Gamma 2 \mu D_\Gamma \mathbf{u} : D_\Gamma \mathbf{v} - \int_\Gamma \pi_s \nabla_\Gamma \cdot \mathbf{v} \end{aligned} \tag{8}$$

In differential form the surface-differential operator associated to the bilinear form above is the tangential counterpart of the Stokes operator. It was introduced by [Scriven \(1960\)](#) and is sometimes referred to as *Boussinesq-Scriven operator*.

2.2 Variational formulation

The Canham-Helfrich energy (1) depends on the shape of Γ and is thus affected by motions along a virtual velocity field \mathbf{v} , unless \mathbf{v} is purely tangential.

A useful expression of the derivative of \mathcal{E} along \mathbf{v} was introduced by [Bonito et al. \(2010\)](#) and reads:

$$d\mathcal{E}(\mathbf{v}) = c_{\text{CH}} \int_\Gamma \left[(\mathbb{I} - 2 \mathbb{P}) \nabla_\Gamma \mathbf{v} : \nabla_\Gamma \boldsymbol{\kappa} + \frac{1}{2} (\nabla_\Gamma \cdot \mathbf{v}) (\nabla_\Gamma \cdot \boldsymbol{\kappa}) \right], \tag{9}$$

where $\boldsymbol{\kappa} = \kappa \check{\mathbf{n}}$. The vector curvature can be defined intrinsically as the surface Laplacian of the function $\boldsymbol{\chi}$ (the identity, i.e., $\boldsymbol{\chi}(\mathbf{x}) = \mathbf{x}$, $\forall \mathbf{x} \in \Gamma$). It satisfies

$$-\nabla_\Gamma \cdot (\nabla_\Gamma \boldsymbol{\chi}) = \boldsymbol{\kappa}. \tag{10}$$

According to the virtual work principle, the virtual work of the viscous stresses plus the virtual change in the energy of the system must equal the virtual work of the internal pressure p of the fluid enclosed by the membrane, i.e., for all \mathbf{v}

$$\mathcal{W}((\mathbf{u}, \pi_s), \mathbf{v}) + d\mathcal{E}(\mathbf{v}) = p \int_{\Gamma} \mathbf{v} \cdot \check{\mathbf{n}}, \quad (11)$$

which, coupled to the inextensibility condition and the compatibility condition (10) ends up giving the following variational problem:

“Find $(\mathbf{u}, \pi_s, \boldsymbol{\kappa}) \in \mathbf{V} \times Q \times \mathbf{K}$ such that

$$\int_{\Gamma} 2\mu D_{\Gamma} \mathbf{u} : D_{\Gamma} \mathbf{v} + \int_{\Gamma} \beta \mathbf{u} \cdot \mathbf{v} - \int_{\Gamma} \pi_s \nabla_{\Gamma} \cdot \mathbf{v} + c_{CH} \int_{\Gamma} \left[(\mathbb{I} - 2\mathbb{P}) \nabla_{\Gamma} \mathbf{v} : \nabla_{\Gamma} \boldsymbol{\kappa} + \frac{1}{2} (\nabla_{\Gamma} \cdot \mathbf{v}) (\nabla_{\Gamma} \cdot \boldsymbol{\kappa}) \right] = p \int_{\Gamma} \mathbf{v} \cdot \check{\mathbf{n}} \quad \forall \mathbf{v} \in \mathbf{V} \quad (12)$$

$$\int_{\Gamma} \xi \nabla_{\Gamma} \cdot \mathbf{u} = \frac{1}{\mathcal{A}} \frac{d\mathcal{A}}{dt} \int_{\Gamma} \xi \quad \forall \xi \in Q \quad (13)$$

$$\int_{\Gamma} \boldsymbol{\kappa} \cdot \boldsymbol{\zeta} = \int_{\Gamma} \nabla_{\Gamma} \boldsymbol{\chi} : \nabla_{\Gamma} \boldsymbol{\zeta} \quad \forall \boldsymbol{\zeta} \in \mathbf{K} \text{ ”.} \quad (14)$$

Here, the internal pressure p is considered given. Alternatively, it can be computed from a volume restriction. The second term in (12) which contains β corresponds to a regularizing friction-like term that filters out rigid-body motions and possible vanishing-stiffness modes. Notice that \mathcal{A} is the area of the membrane ($\mathcal{A} = \text{meas}(\Gamma)$) and that $d\mathcal{A}/dt$ can be chosen arbitrarily to control the total area.

The evolutionary problem reads: Given $\Gamma(0)$, the initial surface, compute a continuous family of surfaces $\Gamma(t)$ and a time dependent velocity field $\mathbf{u}(\cdot, t)$ defined on $\Gamma(t)$, such that at each instant (12)-(14) for some $\pi_s(\cdot, t)$ and some $\boldsymbol{\kappa}(\cdot, t)$, which are subproduct of the calculation. The pair $(\Gamma(t), \mathbf{u}(\cdot, t))$ must still satisfy the *kinematical* condition that the surface Γ moves according to the velocity field \mathbf{u} , or, in mathematical terms, that

$$\forall \mathbf{x} \in \Gamma(t), \text{ dist}(\mathbf{x} + \mathbf{u}(\mathbf{x}, t) \delta t, \Gamma(t + \delta t)) \leq C \delta t^2 \quad (15)$$

where dist stands for the distance between a point and a surface.

3 DISCRETE FORMULATION

The discrete formulation aims at determining the evolution of Γ , from time t_n to time $t_{n+1} = t_n + \delta t$, by computing a velocity field \mathbf{u}_h^{n+1} defined on Γ^n such that Γ^{n+1} is determined by the (Lagrangian) updated nodal positions $\mathbf{X}^{J,n+1}$ (J nodal index), where

$$\mathbf{X}^{J,n+1} = \mathbf{X}^{J,n} + \delta t \mathbf{u}_h^{n+1}(\mathbf{X}^{J,n}) \quad (16)$$

so that (15) is by construction satisfied.

Substituting into (14) one obtains a linearized first-order-accurate discretization in time as first proposed by Bansch (2001)

$$-\delta t \int_{\Gamma^n} \nabla_{\Gamma} \mathbf{u}_h^{n+1} : \nabla_{\Gamma} \boldsymbol{\zeta} + \int_{\Gamma^n} \boldsymbol{\kappa}_h^{n+1} \cdot \boldsymbol{\zeta} = \int_{\Gamma^n} \nabla_{\Gamma} \boldsymbol{\chi}^n : \nabla_{\Gamma} \boldsymbol{\zeta} \quad (17)$$

which creates a coupling between velocity and curvature. Notice that on Γ^n it holds that $\chi^n(\mathbf{x}) = \mathbf{x}$ and thus $\nabla_\Gamma \chi = \mathbb{P}$.

The linear problem that determines \mathbf{u}_h^{n+1} ends up being: “Find $(\mathbf{u}_h^{n+1}, \pi_h^{n+1}, \boldsymbol{\kappa}_h^{n+1}) \in \mathbf{V}_h \times Q_h \times \mathbf{K}_h$ such that

$$\int_{\Gamma^n} 2\mu D_\Gamma \mathbf{u}_h^{n+1} : D_\Gamma \mathbf{v} + \int_{\Gamma^n} \beta \mathbf{u}_h^{n+1} \cdot \mathbf{v} - \int_{\Gamma^n} \pi_h^{n+1} \nabla_\Gamma \cdot \mathbf{v} + c_{CH} \int_{\Gamma^n} \left[(\mathbb{I} - 2\mathbb{P}) \nabla_\Gamma \mathbf{v} : \nabla_\Gamma \boldsymbol{\kappa}_h^{n+1} + \frac{1}{2} (\nabla_\Gamma \cdot \mathbf{v}) (\nabla_\Gamma \cdot \boldsymbol{\kappa}_h^{n+1}) \right] = p \int_{\Gamma^n} \mathbf{v} \cdot \check{\mathbf{n}} \quad (18)$$

$$\int_{\Gamma^n} \xi \nabla_\Gamma \cdot \mathbf{u}_h^{n+1} = \frac{1}{\mathcal{A}} \frac{d\mathcal{A}}{dt} \int_{\Gamma^n} \xi \quad (19)$$

$$-\delta t \int_{\Gamma^n} \nabla_\Gamma \mathbf{u}_h^{n+1} : \nabla_\Gamma \boldsymbol{\zeta}_h + \int_{\Gamma^n} \boldsymbol{\kappa}_h^{n+1} \cdot \boldsymbol{\zeta} = \int_{\Gamma^n} \mathbb{P} : \nabla_\Gamma \boldsymbol{\zeta} \quad (20)$$

hold $\forall \mathbf{v} \in \mathbf{V}_h, \forall \xi \in Q_h$ and $\forall \boldsymbol{\zeta} \in \mathbf{K}_h$.” Together with (16), this completely defines the fully discrete formulation. Notice that all integrals are performed over the known discrete surface Γ^n .

The area control is performed based on a target area \mathcal{A}^* by setting $d\mathcal{A}/dt = -(\mathcal{A} - \mathcal{A}^*)/\tau$, so that if $\mathcal{A} = \mathcal{A}^*$ the right-hand side of (19) vanishes, and if $\mathcal{A} \neq \mathcal{A}^*$ then \mathcal{A} exponentially approaches \mathcal{A}^* with characteristic time τ (chosen as $10\delta t$).

A stabilization term is also added to (16) to avoid spurious modes of π_h . The adopted technique is the orthogonal subscales method (Codina et al., 2001) in which the surface gradient $\nabla_\Gamma \pi_h$ is projected onto the velocity space.

4 REMESHING

The simulation of very large deformations requires of adaptive meshing techniques in order to maintain the required degree of accuracy during the computations. This step is not only needed to cope with the low quality triangles that appear during the simulation, but also to adjust the spatial resolution in places where surface curvature changes in time. For this purpose we used an automatic discrete surface regriding software (Lohner, 1996).

The process of remeshing starts with a general discrete surface (set of 3D points and triangles), and local surface curvature information (specified at the points), which is provided by the field solver. Background sources specifying the desired element sizes are generated at the barycenter of the surface triangles. The desired local element size is computed using the curvature information by the rule $e_h = \alpha r_c$, where e_h is the desired element size and r_c is the radius of curvature. In this study α was set to 0.1 for all the simulations. The specified element size is isotropic since only scalar curvature information is used. The regriding procedure starts by defining one discrete patch as the whole original discrete surface whose boundary is the largest edge of the original mesh. Using this edge as the initial front, the discrete patch is triangulated using an advancing front technique, where new points are projected onto the original discrete surface. A full description of the method together with several techniques for dealing with complex surface geometries can be found in (Lohner, 1996). The output of this step is a completely new discrete surface.

Although the new discrete surface lies on top of the original given surface, there are discrepancies in the curvature calculation when compared with the original mesh. This introduces spikes in the internal energy calculation. However these perturbations are rapidly dissipated, which seems to indicate that do not have an impact on the simulation outcome. The remeshing strategy in this preliminary study is fixed as “remesh every one hundred steps”. Strategies based on element size and quality are currently under investigation.

5 NUMERICAL RESULTS

A tether develops when pulling a parcel of membrane away. If a force F is applied, a structure will develop composed of a head, a cylindrical tube of length $L(t)$ and radius $R(t)$ and the connection to the membrane body as shown in Figure 1.

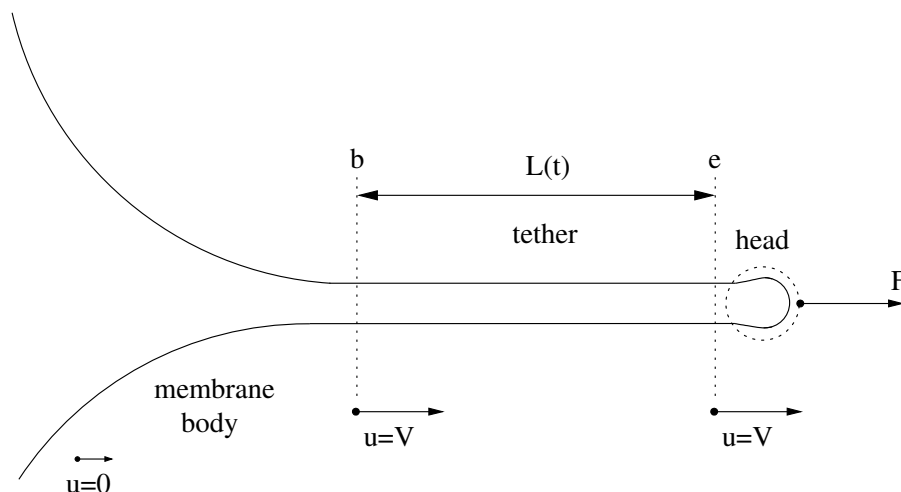


Figure 1: Schematics of membrane tethering.

The dynamics of the tether can be understood with the help of the analytical solution corresponding to a (circular) cylindrical membrane of surface viscosity μ and Canham-Helfrich's constant c_{CH} that is being pulled from its end by an external axial force F . In this particular geometry, the exact problem admits an analytical solution with uniform (independent of x) circumferential and axial stresses. The exact velocity field is given by

$$\mathbf{u} = U_r \check{\mathbf{e}}_r + \gamma z \check{\mathbf{e}}_z \quad (21)$$

with U_r and γ given by

$$U_r = -\frac{1}{8\pi\mu} \left[F - 2\pi c_{\text{CH}} \frac{1}{R} \left(1 + \frac{p R^3}{c_{\text{CH}}} \right) \right], \quad (22)$$

$$\gamma^{\lambda \rightarrow \infty} = \frac{1}{8\pi\mu R} \left[F - 2\pi c_{\text{CH}} \frac{1}{R} \left(1 + \frac{p R^3}{c_{\text{CH}}} \right) \right]. \quad (23)$$

Neglecting the contribution of the internal pressure p , and noticing that

$$\frac{dR}{dt} = U_r \quad (24)$$

one arrives at the more tractable equation

$$\frac{dR}{dt} = \frac{c_{\text{CH}}}{4\mu} \left(\frac{1}{R_{\text{eq}}} - \frac{1}{R(t)} \right). \quad (25)$$

There exists an *equilibrium radius* R_{eq} given by

$$R_{\text{eq}} = \frac{2\pi c_{\text{CH}}}{F}, \quad (26)$$

to which the cylinder will tend as $t \rightarrow \infty$. At equilibrium, the surface tension π_s takes the value

$$\pi_{s,eq} = -\frac{F}{4\pi R_{eq}} = -\frac{F^2}{8\pi c_{CH}}$$

Further, the final decay when $R \simeq R_{eq}$ must have the asymptotic behavior

$$R(t) = R_{eq} + C \exp\left(-\frac{c_{CH}}{4\mu R_{eq}^2} t\right). \tag{27}$$

The characteristic relaxation time is

$$\tau = \frac{4\mu R_{eq}^2}{c_{CH}}$$

For t much greater than τ the tether is expected to be at equilibrium following a rigid-body translation along the line of F . The material deforms to take the shape of a cylinder in the region to the left of point “b” in Figure 1, which is approximately fixed in space (the “beginning” of the tether). Once the material enters the tether it simply moves at constant velocity along it. The “end” of the tether (point “e”) moves at a constant velocity V determined by a balance between the applied force and the viscous stresses at the connection region between the tether and the membrane body.

Numerical simulations were performed pulling a small parcel of an originally spherical membrane of radius 1. The adopted constants were $c_{CH} = 10^{-3}$, $\mu = 1$ and $F = 2\pi$. This corresponds to $R_{eq} = 10^{-3}$, $\pi_{s,eq} = -500$ and $\tau = 0.004$. The friction coefficient β was set to 10^{-2} everywhere except at the bottom of the sphere, where it was set to 100 to serve as a fixation. The time step variable, computed from

$$\delta t = \frac{h_{min}^n}{10\|\mathbf{u}_h^n\|_{max}},$$

where h_{min}^n is the minimum edge length at time t_n and $\|\mathbf{u}_h^n\|_{max}$ the maximum absolute velocity at time t_n .

A sequence of snapshots of the geometrical evolution can be seen in Figure 2, where the colours are assigned to the surface according to the local mean curvature κ_h , for times $t = 1.2 \times 10^{-2}$, 2.9×10^{-2} , 4.7×10^{-2} and 5.5×10^{-2} . Notice that the simulation time corresponds to approximately 14τ , so that an equilibrium tether is expected by the latter times of the simulation.

The profile of the tether as reconstructed from the surface mesh at several instants (once the tether is formed) can be observed in Figure 3. The obtained tether clearly is tending towards its analytic equilibrium value of $R_{eq} = 10^{-3}$. Further, in Figure 4 we plot $R(t) - R_{eq}$ as a function of time as obtained from the 3D simulation for two different values of the viscosity, $\mu = 1$ and $\mu = 2$. The two runs were started from an initial condition which already had an incipient tether and the simulation time was reset to zero, so that the time axis of Figure 4 does not correspond to the instants shown in Figure 3. The relaxation curves in Figure 4 are compared to the exact solution of (25), as obtained by numerical integration with a very small time step. The agreement of the overall dynamics of the 3D tether with the exact solution of the idealized cylindrical tether is quite remarkable, indicating that the fundamental relaxation processes are adequately captured.

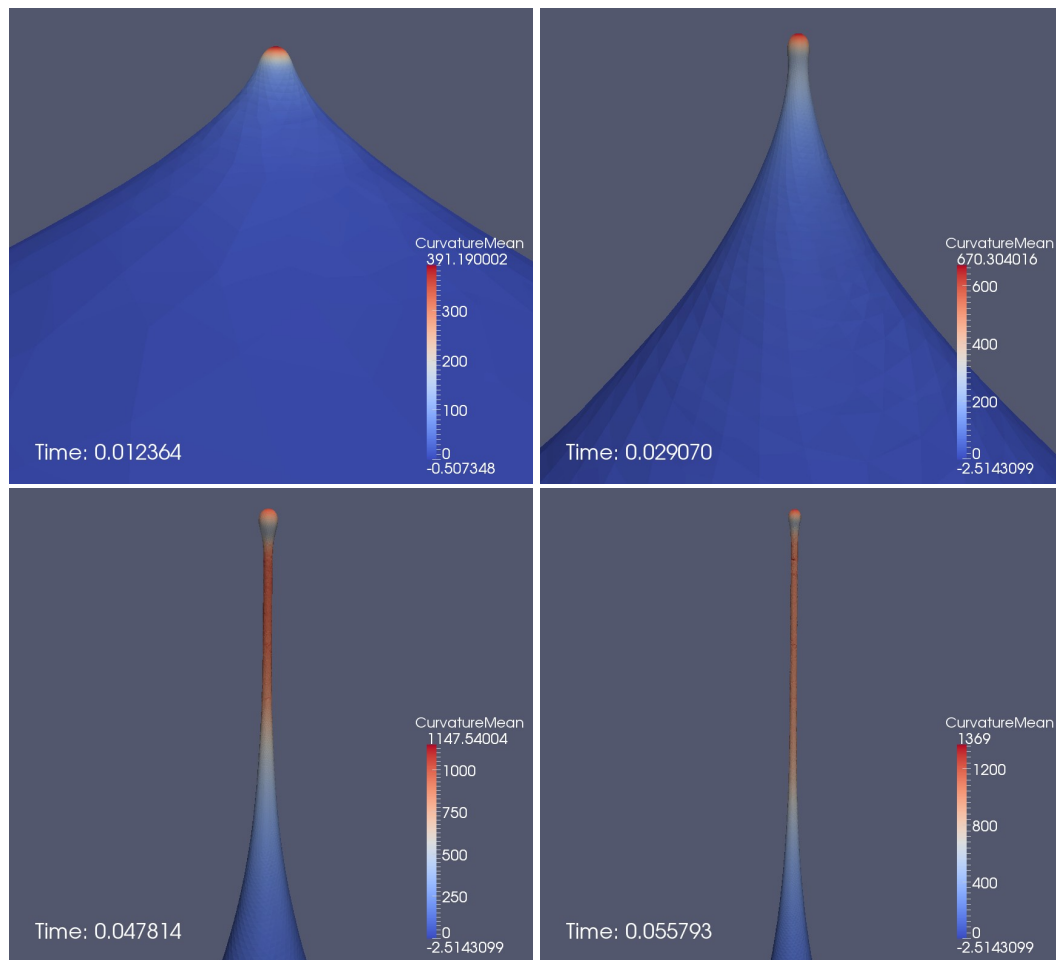


Figure 2: Snapshots of the simulation result. The tether can be identified after $t \simeq 0.029$.

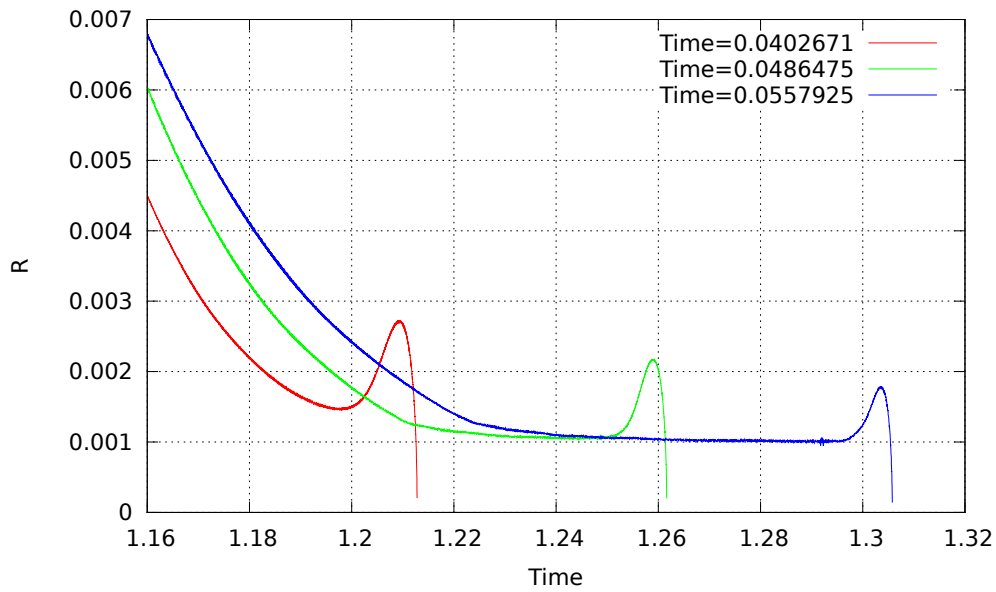


Figure 3: Profile of the simulated tether at several instants. Notice how a cylindrical region with $R \simeq R_{eq}$ spontaneously develops.

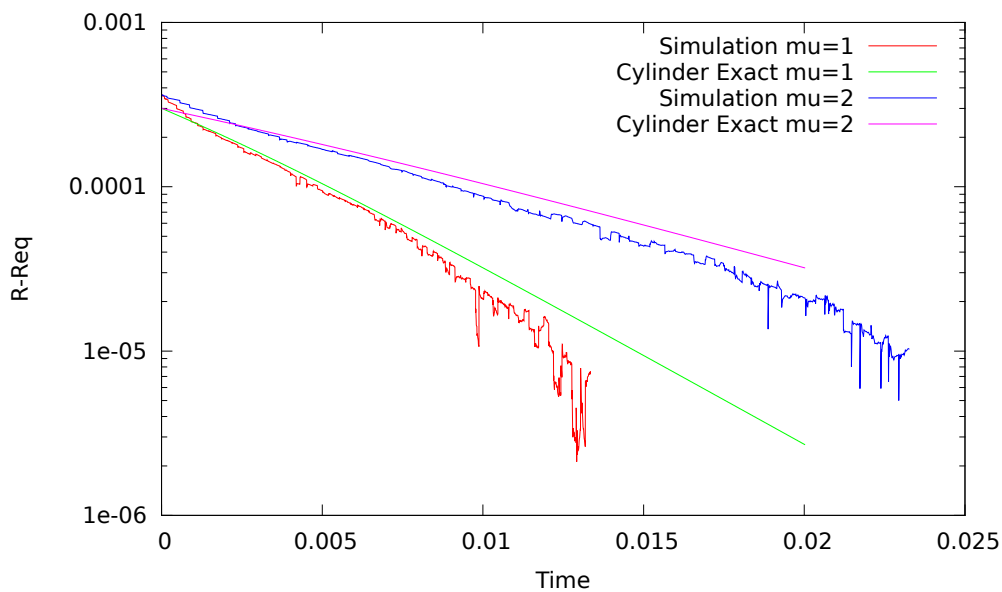


Figure 4: Snapshots of the simulation result. The tether can be identified after $t \simeq 0.029$.

The surface tension π_h at time $t = 0.0557$ is shown as colours on the surface in Figure 5. It can be seen that practically all the cylindrical region has $\pi_h \simeq \pi_{s,eq}$, as expected.

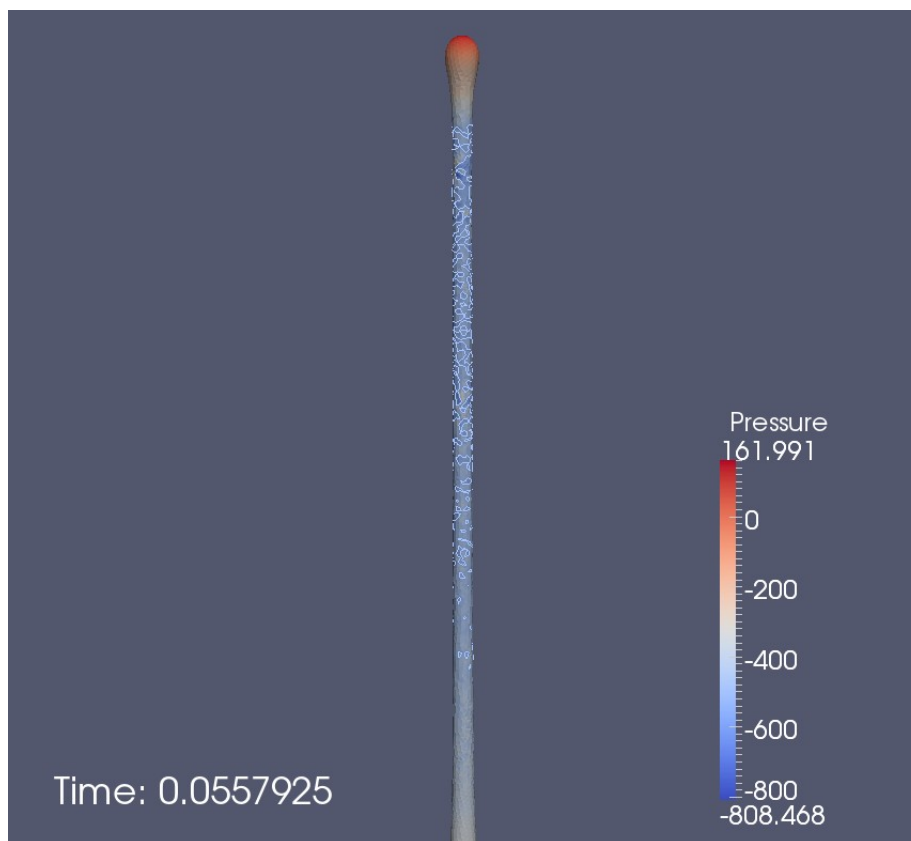


Figure 5: The surface tension π_h at the final time. The white lines correspond to the contour $\pi_h = -500$, which coincides with the equilibrium value $\pi_{s,eq}$.

Figure 6 shows three snapshots taken at different times from a simulation where the discrete surface is left without any remeshing strategy during several hundreds of time steps. It is clear from the pictures that the large deformation process rapidly takes its toll on the surface triangulation if sufficient care is not taken.

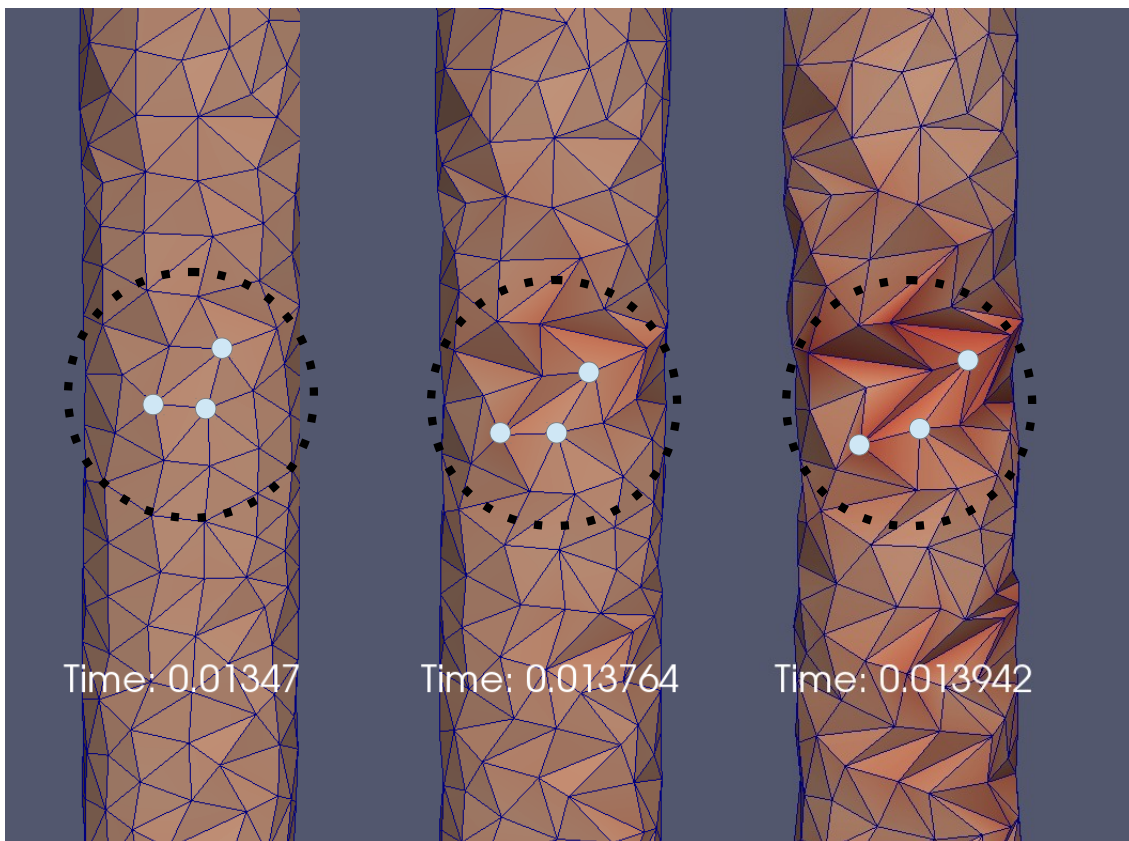


Figure 6: Degradation of the mesh quality if no remesh operation is performed.

6 CONCLUSIONS

In this contribution, we have introduced a fully discrete semi-implicit finite element scheme for the simulation of viscous membranes with bending elasticity of the Canham-Helfrich type. The scheme has been applied to the phenomenon of tether formation. The first preliminary results reported above are encouraging as compared to analytical results of an idealized cylindrical tether. Still, the algorithm exhibits some type of weak instability that makes it mandatory to use quite small time steps and frequent remeshing. Further investigations are under way to increase the robustness of the method.

ACKNOWLEDGMENTS

Partial financial support from FAPESP (Brazil), CNPq (Brazil) and INCT-MACC (Brazil) is gratefully acknowledged.

REFERENCES

- Alberts B., Bray D., Hopkin K., Johnson A., Lewis J., Raff M., Roberts K., and Walter P. *Essential Cell Biology*. NY Garland Science, New York, 2010.
- Bänsch E. Finite element discretization of the Navier–Stokes equations with a free capillary surface. *Numer. Math.*, 88:203–235, 2001.
- Bonito A., Nochetto R.H., and Pauletti M.S. Parametric FEM for geometric biomembranes. *Journal of Computational Physics*, 229(9):3171–3188, 2010.

- Bozic B., Svetina S., and Zeks B. Theoretical analysis of the formation of membrane microtubes on axially strained vesicles. *Phys. Rev. E*, 55:5834–5842, 1997.
- Canham P. The minimum energy of bending as a possible explanation of the biconcave shape of the human red blood cell. *J. Theor. Biol.*, 26:61–81, 1970.
- Codina R., Blasco J., Buscaglia G.C., and Huerta A. Implementation of a stabilized finite element formulation for the incompressible Navier-Stokes equations based on a pressure gradient projection. *International Journal for Numerical Methods in Fluids*, 37(4):419–444, 2001.
- Gross S. and Reusken A. *Numerical Methods for Two-phase Incompressible Flows*,. Springer Series in Computational Mathematics, Vol. 40, 2011.
- Harland C., Bradley M., and Parthasarathy R. Phospholipid bilayers are viscoelastic. *Proc. Nat. Acad. Sci. USA*, 107:19146–19150, 2010.
- Harland C., Bradley M., and Parthasarathy R. Retraction. *Proc. Nat. Acad. Sci. USA*, www.pnas.org/cgi/doi/10.1073/pnas.1111381108, 2011.
- Helfrich W. Elastic properties of lipid bilayers – theory and possible experiments. *Zeitschrift für Naturforschung C*, 28:693–703, 1973.
- Lee H.J., Peterson E.L., Phillips R., Klug W.S., and Wiggins P.A. Membrane shape as a reporter for applied forces. *Proceedings of the National Academy of Sciences*, 105(49):19253–19257, 2008. doi:10.1073/pnas.0806814105.
- Lohner R. Regridding surface triangulations. *Journal of Computational Physics*, 126(1):1 – 10, 1996.
- Scriven L. Dynamics of a fluid interface. equations of motion for newtonian surface fluids. *Chem. Eng. Sci.*, 12:98–108, 1960.
- Smith A.S.c.v., Sackmann E., and Seifert U. Pulling tethers from adhered vesicles. *Phys. Rev. Lett.*, 92:208101, 2004. doi:10.1103/PhysRevLett.92.208101.
- Waugh R. Surface viscosity measurements from large bilayer vesicle tether formation I: analysis. *Biophys. J.*, 38:19–27, 1982a.
- Waugh R. Surface viscosity measurements from large bilayer vesicle tether formation II: experiments. *Biophys. J.*, 38:29–37, 1982b.
- Willmore T.J. *Riemannian Geometry*. Clarendon Press, Oxford, 1993.